Laboratory investigation of the temperature influence on the mechanical properties and fracture crack distribution of rock under uniaxial compression test

Weijing Xiao[1,2] · Dongming Zhang[1,2] · Han Yang[1,2] · Xiaoming Li[1,2] · Maolin Ye[1,2] · Shujian Li[1,2]

Abstract

In order to study the influence of high temperature on the mechanical characteristics and crack distribution of progressive failure process of rock, the laboratory uniaxial compression experiments were carried out on sandstone treated with different temperatures (25–1000 °C), and the variation characteristics of stress, deformation, and acoustic emission parameters during the failure of samples were analyzed. At the same time, the fracture crack distribution and fractal characteristics were analyzed through the industrial computed tomography (CT) test of the failure samples. The results show that temperature can affect the deformation and strength characteristics of rock. The stress thresholds and elastic modulus appear to increase when the preheating temperature increases from 25 to 400 °C and decrease when greater than 400 °C. The activity of AE signal is positively correlated with temperature. The CT results confirmed that with increasing temperature, the fracture cracks in the failure samples changed from a small number of single fracture cracks to a complex and crisscross distribution of small cracks. The failure cracks gradually gathered in the middle of the samples. The box-counting dimension of the fracture crack is between 1.4060 and 1.7262, and higher preheating temperature corresponds to the larger box-counting dimension, indicating that the temperature increases the complexity of the fracture crack. This outcome shows that temperature has an important influence on the deformation and failure of rock.

Introduction

Rock masses are natural geological bodies formed by long geological tectonic movements in nature, and they are the main material component of crust and mantle (Koprubasi and Aldanmaz 2004; Ao et al. 2010; Singh 2019). Rock is a solid polymer composed of a variety of minerals and is an important material for human survival. It is widely used in water conservancy, hydropower, civil engineering, mine development, nuclear waste storage, urban underground space, and many other industries (Feng et al. 2019; Gong et al. 2019a, b; Yang et al. 2019; Chen et al. 2019a, b). Along with the exploration of mining resources, the stability monitoring and prediction of roadway engineering designs after disasters, such as deep coal spontaneous combustion and roadway fire, are the main engineering problems currently being encountered (Araújo et al. 1997; Yang 2015; Zhang et al. 2015; Yang et al. 2017). Therefore, the mechanical properties of rock after high temperature play an important role in the stability of rock engineering. The research results can provide reference for the selection of engineering structural parameters, scientific management, and stability evaluation.

Considering the influence of temperature on the stability of rock mass engineering, many scholars take the rock after high temperature as the research object and use the method of experimental research and numerical calculation to carry out a lot of research work and have achieved fruitful results. Peng et al. (2019) studied the acoustic emission characteristics of marble with different thermal damage degrees and sizes during rock failure process. In order to explore the influence of

✉ Dongming Zhang
  zhangdm@cqu.edu.cn

1   State Key Laboratory of Coal Mine Disaster Dynamics and Control, Chongqing University, Chongqing 400044, China

2   School of Resources and Safety Engineering, Chongqing University, Chongqing 400044, China

different temperature and cooling methods on the physical and mechanical properties of Sandstone during stress-strain process, Rathnaweera et al. (2018) carried out uniaxial compression test on the sandstone after heat treatment. The results show that temperature can affect the mechanical properties, mineral composition, and microstructure of rock and the cooling methods can change the elastic modulus and fracture characteristics of rock. Rao et al. (2007) carried out mechanical tests on sandstone after different high-temperature treatments and studied the physical and mechanical parameters of rock after high temperature. The test results indicate that the strength parameters of sandstone first increased and then decreased linearly with increasing temperature. Liu and Xu (2015) carried out indoor physical and mechanical tests on sandstone and granite treated at different temperatures and studied the effects of physical and mechanical properties of rocks at different temperatures. Their study found that the temperature can affect the mechanical and physical properties of rock, but the physical properties are more dependent on the temperature than the mechanical properties. To study the dynamic response characteristics of rocks to impact loads after different thermal damage treatments, Chen et al. (2014) conducted indoor dynamic load mechanics experiments with sandstone as the research object, and the results showed that the dynamic deformation and mechanical properties of rock were affected by both temperature and impact load. In addition, some researchers have realized the impact of high-temperature heat treatment on rocks and carried out considerable research work (Xie et al. 2015; Song et al. 2018; Gaunt et al. 2016; You et al. 2018; Zhao et al. 2017).

It is noteworthy that the fracture behavior and the post-high-temperature rock material play an important role in geotechnical engineering. The CT technology and scanning electron microscope (SEM) technology are the main technical means to study the micro-cracks of rock fracture. In order to study the characteristics of rock fracture and seepage after high-temperature damage, Chen et al. (2019a) carried out seepage tests under different seepage pressures on rocks after high temperature and monitored the internal fracture opening of rock samples after test based on CT scanning technology. Wang et al. (2020) used CT technology to study the thermal fracture of shale after 20–600 °C treatment, revealing the internal reasons for the anisotropy of shale permeability changing with temperature. Saif et al. (2017) and Rabbani et al. (2017) used CT technology to study the evolution process of shale pores and fractures under high temperature. By conducting laboratory mechanical tests and SEM tests on sandstone, Zhang et al. (2018) obtained the stress-strain data of the progressive failure process of sandstone treated with different temperatures and the microscopic fracture morphologies of the rock under different temperatures. The results show that under the influence of temperature, the cracks in rock have obvious deformation, especially when the temperature reaches 400 °C; the

thermal damage cracks are obvious. In order to analyze the changes of macromechanics and microstructure in the process of cyclic heating and cooling of rock, Liu et al. (2017) carried out uniaxial compression test on the sandstone after high-temperature treatment and used acoustic emission test, acoustic wave test, and electron microscope scanning test methods. The research shows that the rock mineral composition decomposes, microcracks expand, sample integrity, and strength degradation after the influence of thermal stress. The existing research results have been reported in detail about the mechanism of strength failure and crack evolution in the process of rock deformation and failure after different temperature treatments, and these studies can be used for reference to further study the mechanical and damage characteristics of rock after high-temperature damage. However, it is not enough to limit our understanding, and it is more necessary to understand the characteristic stress parameters and fractal characteristics of fracture cracks under the influence of high temperature.

This investigation attempts to use indoor experiments to analyze the physical and mechanical characteristics of rock after high-temperature treatment, as well as the distribution characteristics of the interrupted crack of the sample. First, put the rock samples into resistance furnace and heat them to different temperatures, and keep the constant temperature for 4 h and naturally cooled. Then, a uniaxial compression test was carried out on the samples, and an acoustic emission detection system was used to collect and record the acoustic emissions during the test. Finally, the thermally damaged samples were scanned by CT to study the distribution characteristics of the fracture cracks in them based on the influence of temperature. The results can be used as references for the study of rock mechanics with the influence of temperature.

Experimental program and equipment

Sample preparation

The rock samples are from Jiangbei District in Chongqing, China. These rocks are naturally bluish gray in color, with uniform texture and few cracks. The main minerals are quartz, feldspar, mica, calcite, clay, and other mineral components. The average density is 2.35 g/cm3. The average initial porosity of the sample is 7.195%, and the pore size distribution is shown in Fig. 1.

In order to reduce the test error, drilling and sampling are carried out on the same rock block, and rock samples with uniform texture and no obvious cracks are selected to be processed into cylindrical standard samples of φ50 × 100 mm. In order to make the surface flatness of the sample within ±0.02 mm and the parallelism within ±0.05 mm, the machining process mainly includes cutting and grinding. All of the cylindrical standard samples were divided into six groups, one

Fig. 1 Test material: (**a**) sampling location, (**b**) pore size distribution, and (**c**) heated sandstone samples
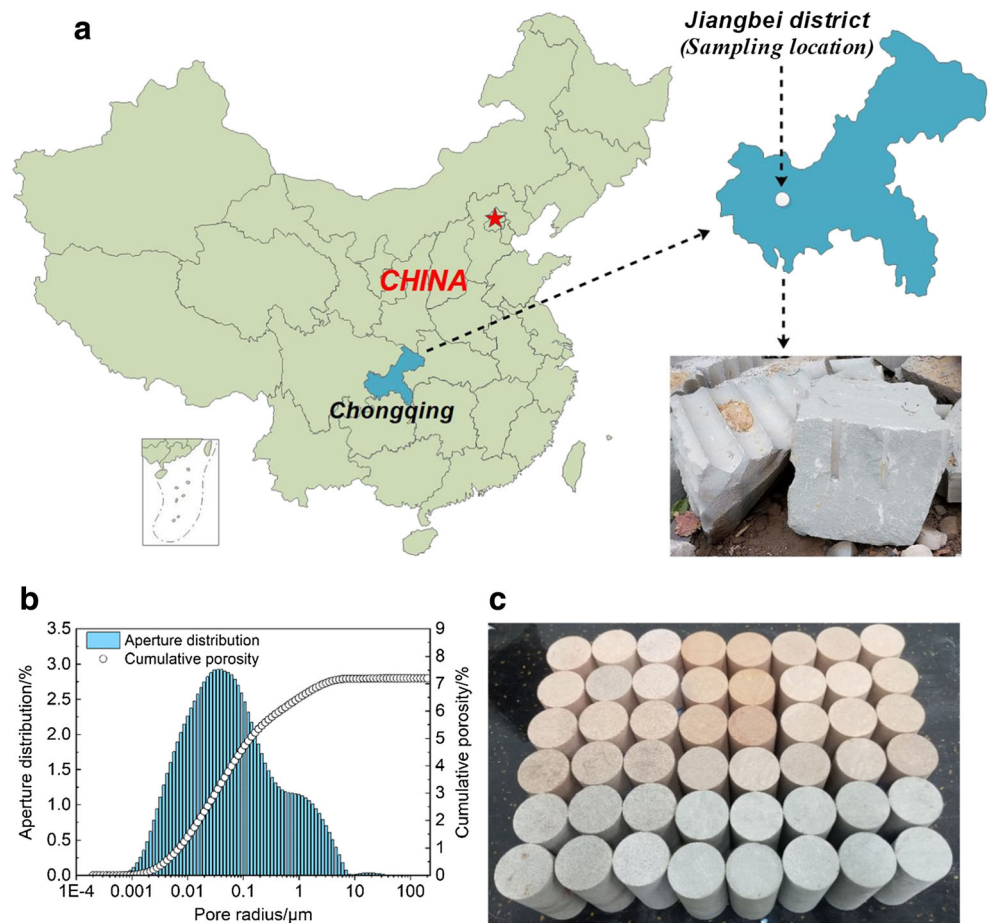
of which was not heated (T = 25 °C), and the remaining groups were put into resistance furnace for high-temperature treatment at different temperatures (T = 200, 400, 600, 800, and 1000 °C) with a heating rate of 10 °C/min. After reaching the set temperature, samples were kept in the resistance furnace with a constant temperature for 4 h and then cool down naturally in the box-type electric resistance furnace. The samples are as shown in Fig. 1(c). The box-type electric resistance furnace (SX₂–10-12A) is made in Shaoxing, China, and the highest temperature is 1200 °C.

Experimental equipment

The experimental equipment, as shown in Fig.2. The stress loading system is the Shimadzu AG-IS material testing machine (AG-250 kN IS). The main parameters of the equipment are as follows: the maximum axial load of the testing machine is 250 kN, the loading rate ranges from 0.0005 to 1000 mm/s, and the minimum sampling interval is 1.25 ms. In order to reduce friction, it is necessary to apply appropriate amount of Vaseline on both ends of the sample. The data acquisition system comprises the ASMD3–16 high-speed dynamic resistance strain gauge and the PCI-2 AE monitoring system. The ASMD3–16 high-speed dynamic resistance strain gauge is a high-

performance product independently developed by Ji'nan Sigma Company (China). By attaching strain gauges onto the surface of samples, it can monitor and preserve the deformation of samples during uniaxial compression in real time. The PCI-2 AE monitoring system was used to monitor the acoustic emission signal during the failure process of the sample, and the threshold for detection was 45 dB. In order to prevent the test failure caused by the damage of acoustic emission sensors during the test, two acoustic emission sensors are selected to collect the acoustic emission signals during the test. The two sensors are respectively installed on the opposite surface in the middle of the sample, which are both fixed with rubber rings. The AE signal was preamplified (40 dB) and transferred to the PCI-2 AE monitoring system. Before the experiment began, a suitable amount of Vaseline should be applied to the contact position between the sensor and the sample.

Results

Results of mechanical tests

Peak stress and elastic modulus are two important parameters for characterizing the mechanical properties of rock. The

Fig. 2 Experimental equipment
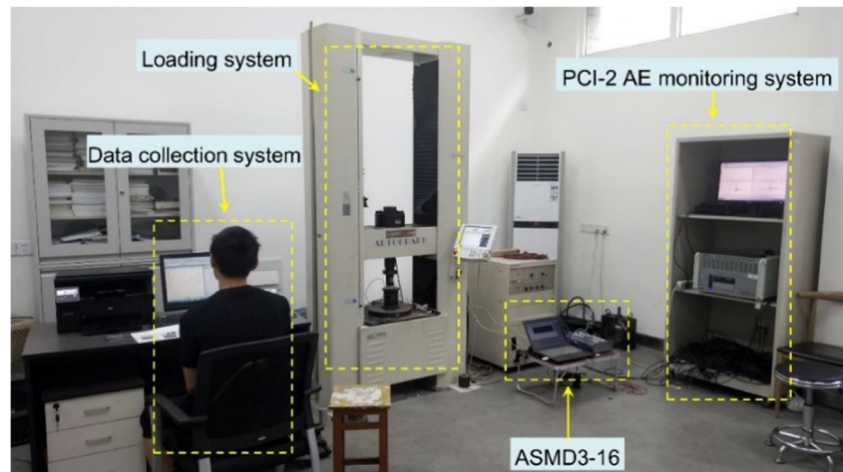
moving point linear regression method can be used to determine the elastic modulus of different samples during the deformation process under the axial loading (Xiao et al. 2020), which the author will not repeat. Figure 3 is the stress-strain curve of progressive failure process of rock after different temperature treatments and the relationship curve of peak stress, elastic modulus, and temperature. According to Fig. 3(a), there are some differences in the stress-strain curves of the sandstone samples during the failure process at the different temperatures. When the pretreatment temperature was 25–400 °C, the stress-strain curves of each sample were almost identical except for the different peaks. During the deformation process, the elastic modulus increased slightly with increasing temperature, as shown in Fig. 3 (b), and the deformation modulus increased from 14.8 to 15.8 GPa, which is an increase of 6.7%. Compared with the elastic modulus, the peak stresses increased from 63.5 to 93.7 MPa, which is an increase of 47.6%. With increasing temperature, the peak stresses increased at a considerable rate. Conversely, it can be seen from Fig. 3(a), when the pretreatment temperature exceeds 400 °C, the stress-strain curves are quite different, and the elastic modulus of the rocks decreases rapidly with

increasing temperature. The deformation modulus decreased rapidly from 15.8 to 5.3 GPa, with a decrease of 66.5%, as shown in Fig. 3(b). In addition, the peak strength of the sandstone samples decreases rapidly with the increase in temperature, as shown in Fig. 3(b), and with the increase in temperature, the peak strength decreases from 93.7 to 33.7 MPa, with a decrease of 64.0%.

The above experimental results show that the rocks treated at different temperatures have different mechanical properties, mainly in the following aspect that with the temperature increase, the peak strength and elastic modulus first increase and then decrease, in which 400 °C is the critical temperature, when the temperature is lower than 400 °C, the mechanical properties of rocks are strengthened, and when the temperature is higher than 400 °C, the mechanical properties of the rocks are degraded.

Strength and deformation characteristics

Progressive rock failure is a process in which the rock gradually changes from "elastic" to "damaged" and finally "fractured" (Lv et al. 2018). Therefore, studying the internal crack
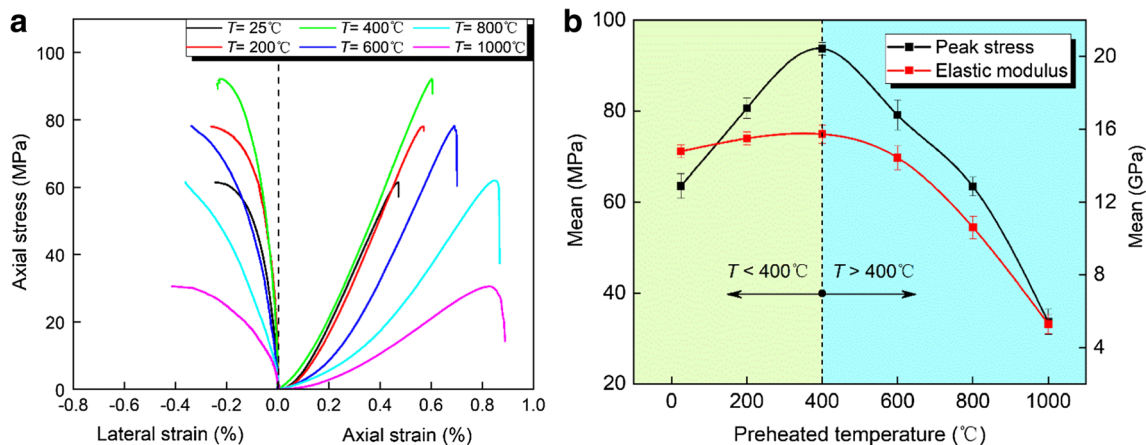

Fig. 3 Test data curves: (**a**) the typical stress-strain curves for tested specimens and (**b**) peak stress and elastic modulus

evolution during the rock failure process is conducive to an accurate understanding of the progressive rock failure process. Martin (1997) and Eberhardt (1998) divided the process of progressive rock failure into five stages according to the evolution law of the volume strain and crack volume strain of the rock samples during the process of progressive failure, which are the crack closure stage, elastic stage, stable crack growth stage, unstable crack growth stage, and post peak stage, and the corresponding stress value in each stage is called the stress eigenvalue. In this paper, according to the generalized Hooke law, the volume strain and crack volume strain during the process of progressive rock failure under uniaxial compression can be calculated as follows according to Eq. (1):

$$\begin{cases} \varepsilon_v = \varepsilon_1 + 2\varepsilon_3 \\ \varepsilon_v^c = \varepsilon_v - \dfrac{1-2\mu}{E}\sigma_1 \end{cases}, \qquad (1)$$

where ε_v and ε_v^c are the rock volume strain and crack volume strain, respectively; ε_1 and ε_3 are the axial strain and radial strain, respectively; μ is Poisson's ratio of the sample; and E is the elastic modulus.

According to Eq. (1), the relationship curves between the volume strain and crack volume strain and the axial stress of rock samples under uniaxial compression were calculated, as shown in Fig. 4. The analysis shows that the rock sample volume and crack volume undergo two distinct processes of compression and expansion after different temperature treatments. The deformation process is analyzed as follows:

At the initial stage of stress loading, both the volumetric strain curve and the volumetric strain curve of the crack appear concave in shape, indicating that the sample volume is gradually compressed and the internal gap cracks are gradually compressed. This stage belongs to the crack closure stage. The corresponding stress value of this stage is the crack closure threshold σ_{cc}, and the crack volume strain increment $\left(\Delta\varepsilon_v^{cc}\right)$ compressed during this stage is the initial crack volume. With the gradual increase in axial stress, the sample volume continues to be compressed; in contrast, the crack volume strain remains the same. This outcome indicates that the initial crack of the rock has been fully compressed and closed during the crack closure phase. When the axial stress exceeds the crack closure threshold σ_{cc}, the rock deformation is derived from the elastic deformation of rock particles; this stage belongs to the elastic deformation stage, and the stress corresponding to this stage is the crack initiation threshold σ_{ci}. When the axial stress exceeds σ_{ci}, the crack inside the specimen begins to expand, the volume strain curve of the crack gradually increases to a negative direction, and the volume of the specimen continues to be compressed. This stage belongs to the stage of stable pore fracture development. The stress value corresponding to this stage is called the crack damage threshold σ_{cd}, and the crack volume strain increment generated during this stage is $\Delta\varepsilon_v^{cd}$. When the stress exceeds σ_{cd}, the internal crack of the sample rapidly increases and passes through, and the sample volume begins to expand until the axial stress reaches the peak stress. This stage belongs to the

Fig. 4 Progressive failure process of rock samples
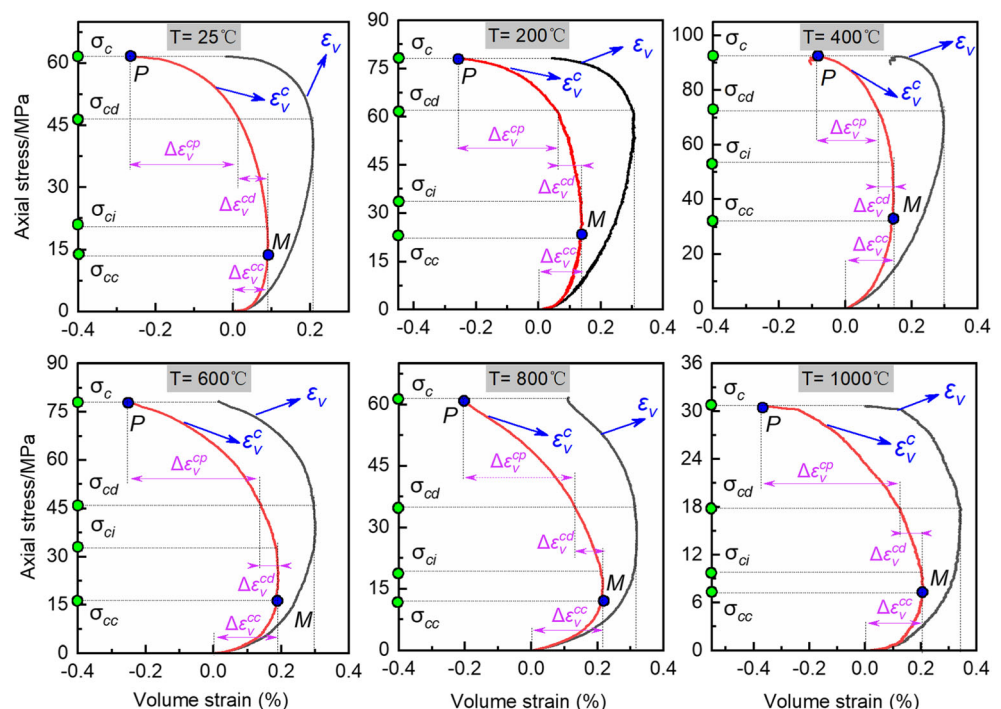
unstable crack development stage, and the crack volume strain increment generated during this stage is $\Delta\varepsilon_v^{cp}$. The stress threshold and crack volume strain increment at each deformation stage of the sample are shown in Fig. 5.

Figure 5 shows that the rock stress characteristic value shows the same change rule with the increase of temperature, that is, with the temperature increase, the stress characteristic value increases first and then decreases. And the same as the results in "Results and deformation characteristics" section, 400 °C is also the critical value of the change curve of rock stress characteristic value, as shown in Fig. 5 (a). When the temperature is 25–400 °C, the stress thresholds increase with the temperature increase, and all of the stress characteristic values of the sample reach the maximum at 400 °C. In addition, compared with the sample at 25 °C, the increases in σ_{cc}, σ_{ci}, σ_{cd}, and σ_c of the rock at 400 °C are 125.7, 156.6, 54.4, and 49.7%, respectively. When the temperature is 400–1000 °C, all the stress thresholds decrease with the temperature increase, and they decrease to the minimum value at 1000 °C. Compared with 400 °C, the reductions of σ_{cc}, σ_{ci}, σ_{cd}, and σ_c are 76.4, 81.9, 75.7, and 66.7%, respectively. These results show that 400 °C is the critical temperature of the sandstone samples, and the stress characteristic values of the rock samples reach the maximum value at this temperature. When the temperature exceeds 400 °C, the stress characteristic values of the samples will gradually decrease. The results show that 400 °C is the critical temperature of sandstone samples and the stress characteristic values of the rock samples reach the maximum value at this temperature. After exceeding this critical temperature, the stress characteristic values of the samples will gradually decrease.

Similar to the stress thresholds, the crack volumetric strain increments of the rock samples at the different deformation stages are also significantly correlated with temperature, as shown in Fig. 5(b). With increasing temperature, the crack volumetric strain increments $\Delta\varepsilon_v^{cc}$ increases gradually during the compaction stage of the rock sample during deformation, indicating that the internal cracks of the rock samples increase after the high-temperature treatment. The crack volumetric strain increment $\Delta\varepsilon_v^{cd}$ generated during the stage of stable crack development is almost constant with increasing temperature, except for slight increases at 400 and 600 °C, indicating that temperature has little influence on crack growth at the stable deformation stage of rock samples under uniaxial compression. Compared with $\Delta\varepsilon_v^{cc}$ and $\Delta\varepsilon_v^{cd}$, the crack volumetric strain increment ($\Delta\varepsilon_v^{cp}$) during the unstable crack development stage is the most obviously affected by temperature, as shown in Fig. 5(b). As the temperature increases, $\Delta\varepsilon_v^{cp}$ first decreases and then increases. When the temperature is 400 °C, $\Delta\varepsilon_v^{cp}$ is the smallest; and when the temperature exceeds 400 °C, $\Delta\varepsilon_v^{cp}$ will gradually increase. The results show that for the unstable crack propagation stage of rock failure process, when the temperature is 25–400 °C, the preheating temperature inhibits crack development; on the contrary, when the temperature exceeds 400 °C, the high temperature can promote crack development.

Fracture crack distribution characteristics

The fracture morphology of rock samples, which are damaged by uniaxial compression after the different temperature treatments, is complex and changeable (Tang et al. 2015; Lu et al. 2016). To more intuitively describe the internal fracture crack and damage structure characteristics of the failure sample, a CT scanner is used to monitor and analyze the sample failure. The CT scanner can clearly and accurately detect the internal defects of the sample and can be used to analyze the damage and failure development process of the internal crack in the rock specimen (Yushi et al. 2016). In this paper, the Siemens CT experimental system was used to reconstruct a CT image of the damaged rock. There are 24 detectors in the CT
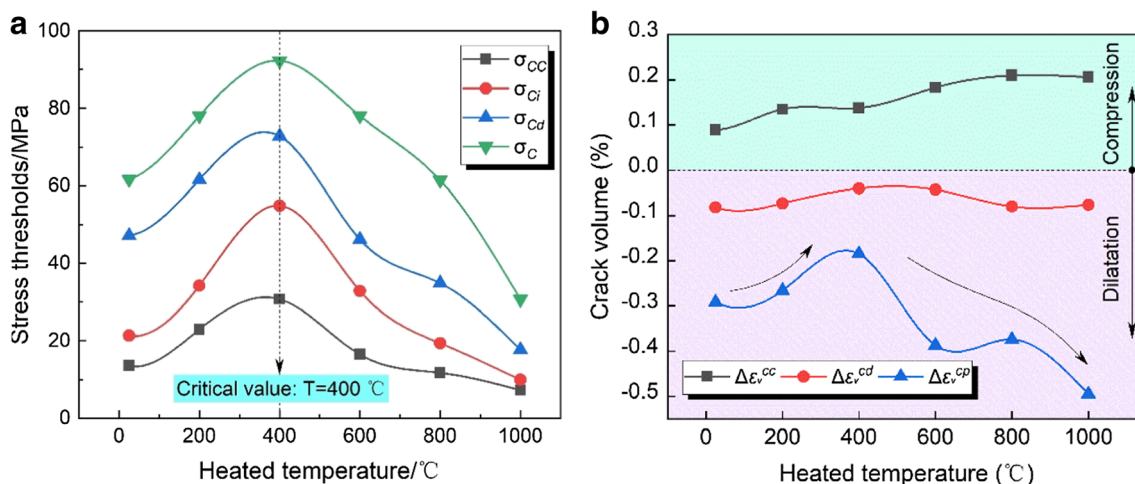

Fig. 5 The stress threshold value and crack volumetric strain increment of the sample heated by the different temperatures (*Note: The negative number represents the crack dilatation, not the numerical size*)

experimental system, with the maximum X-ray bulb current of 345 mA and the maximum X-ray voltage of 130 kV. In the sequential scan mode, the number of uninterrupted scans in each range is 99, and the layer thickness is 0.6–19.2 mm. The reconstructed field of view is ranged from 5 to 50 cm, and the maximum IRS reconstruction rate is 20 images per second. The thickness of the reconstruction was 0.75 mm. According to the reconstructed three-dimensional diagram, the fracture crack morphology and distribution characteristics of the sample could be clearly seen. To study the representative fracture crack distribution inside the sample characteristics, four typical slices are extracted from each sample for analysis. Among them, three typical image slices (slice A, slice B, and slice C) are extracted in the axial direction with equal spacing, one typical image slice is extracted in the diameter direction (slice D), as shown in Fig. 6 (a), and the CT image slice of the rock sample after the uniaxial compression test is shown in Fig. 6. Due to limited space, the paper only lists the CT images of rocks at three different temperatures.

Under normal temperature (25 °C), Fig. 6 shows that the rock samples have simple cracks after the uniaxial compression failure, and the samples are relatively complete, with a small crack density and poor penetration. The fracture crack is composed of two main fracture cracks, and the cracks are mainly distributed near the upper end of the sample. When the fracture crack extends to the lower end, it gradually evolves into several small cracks. Compared with 25 °C, the crack distribution of the specimen after the high-temperature treatment at 400 °C is more complex after the uniaxial compression failure. The main fracture cracks penetrate the two ends of the specimen. From the radial slices A, B, and C, there are many small cracks besides the main fracture cracks, and there are many cracks in the middle of the specimen; in addition, the density and connectivity of the fracture cracks increase. Compared with 25 and 400 °C, the crack distribution complexity of the damaged sample increases obviously when the pretreatment temperature is 800 °C, and the broken degree of the damaged sample also increases obviously. The middle part of the sample has the most cracks and the highest damage degree. In addition, the fracture crack distribution of the failure specimen is characterized by small length, high density, narrow width, and high connectivity. The results show that after a high-temperature treatment, the internal crack growth and connectivity increase obviously, and the damage of the middle part of the specimen is the largest. The spatial distribution of the fracture cracks after uniaxial compression is more complex. The obvious characteristics of the fracture samples are the increase in crack density, connectivity, and fracture degree.
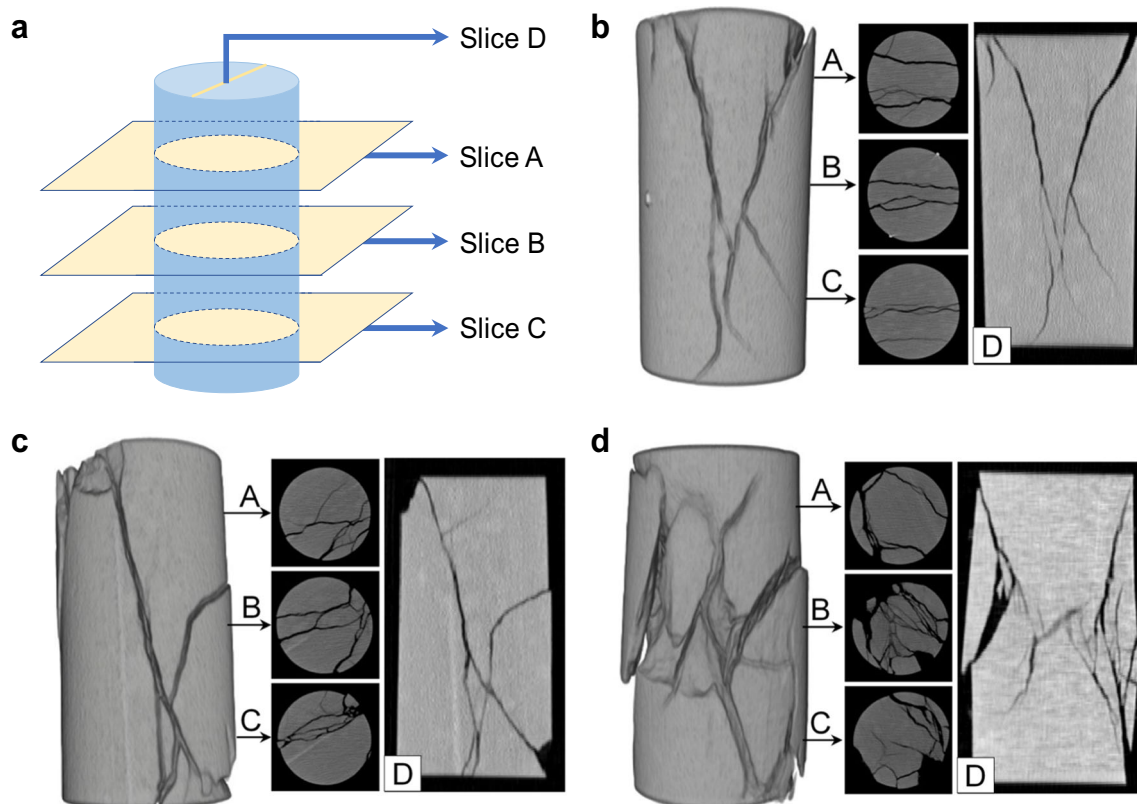
Fig. 6 CT images and image slices of typical damaged samples: (**a**) schematic diagram of slice extraction, (**b**) $T = 25$ °C, (**c**) $T = 400$ °C, and (**d**) $T = 800$ °C

Discussion

AE response characteristics of rock during the progressive failure process

Materials under the action of an external load will produce corresponding deformation; at the same time, the internal energy will be released in the form of elastic waves, which is called acoustic emission (AE) (Ohnaka 1983; Manthei 2005). Because the acoustic emission phenomenon will occur during the progressive failure process of rock under an external load, it is often used to study the change in internal cracks during the failure process of rock masses in the fields of mining engineering, geotechnical engineering, etc., which provides the basis for the disaster control and prediction of engineering rock masses of interest (Cheon et al. 2011; Wang et al. 2017). Acoustic emission (AE) parameter analysis is the most commonly used and direct method of acoustic emission signal analysis. The acoustic emission parameters mainly include the event rate, ringing count rate, energy rate, amplitude, cumulative event number, cumulative ringing count, and cumulative energy. The AE ringing count refers to the number of oscillations of signals above the threshold value; in addition, the number of oscillations per unit time that exceed the threshold signal is called the ringing count rate, which can reflect the damage characteristics of the material. Therefore, in this paper, the AE ringing rate is used to analyze the acoustic emission response characteristics of rock samples under uniaxial compression at different temperatures. Figure 7 shows the evolution characteristics of the ringing count rate during the stress-strain process of samples treated at different temperatures (25–1000 °C).

Compared with rock samples at room temperature (T = 25 °C), the acoustic emission response characteristics of rock samples treated at the different temperatures are significantly different, as shown in Fig. 7. The main trend is as follows: (a) with the increase in temperature, the acoustic emission ringing rate of the samples after the temperature treatment increases significantly at the initial stage of stress loading; (b) compared with the samples at 25, 200, and 400 °C, there is a strong acoustic emission activity observed before the peak stress when the temperature is over 400 °C. It can be seen from the analysis that with increasing temperature, the free water between the rock particles gradually evaporates and escapes, and the internal crack of the sample increases, resulting in crack volume strain increments ($\Delta\varepsilon_v^{cc}$) increasing with increasing temperature (Fig. 5 (b)). Since the acoustic emission phenomenon occurs during the process of pore compaction, the acoustic emission ringing count rate of samples during the initial stress stage after the temperature treatment is significantly higher than that of samples at room temperature, as shown in Fig. 7. When the axial stress gradually approaches the peak stress, the crack volumetric strain increment ($\Delta\varepsilon_v^{cp}$) is the smallest during the unstable crack development stage when the temperature is 400 °C. When the temperature is over 400 °C, $\Delta\varepsilon_v^{cp}$ is rapidly increasing (as shown in Fig. 5 (b)). The crack growth process is accompanied by acoustic emission phenomena. Therefore, compared with the samples at 25, 200, and 400 °C, there are more AE ringing count rates at the unstable crack development stage before the peak stress of the samples occurs when the temperature is higher than 400 °C, as shown in Fig. 7.

Fractal characteristics of the fracture cracks based on CT images

CT image binarization and crack identification

To analyze the fractal dimension characteristics of the fracture crack distribution in the axial direction of the samples, slice D of the CT reconstruction three-dimensional diagram of each sample was selected to identify and extract the fracture cracks in the axial direction based on the experimental results in "Fracture and crack distribution characteristics" section. The CT image obtained from the experiment is gray scale image, and the range of gray value is 0–255. The region with a lower gray scale value is the fracture of the sample obtained by CT scanning, while the region with a higher gray scale value represents the matrix of the sample without fractures. In this paper, the fracture region with low gray scale is selected as the target region for fractal dimension analysis. In order to extract the crack of the sample properly, the judgment function (as show in Eq. (2)) is used to segment each pixel of the gray image, and the gray image is transformed into a binary image. In the binary image, the white area is the sample matrix, and the black part is the crack, which is the target area. Through the above calculation process, the binary images of slice D of typical samples are obtained, and the black area of the image is the extracted fracture crack, as shown in Fig. 8,

$$F(i,j) = \begin{cases} 0, f(i,j) \leq \alpha \\ 1, f(i,j) > \alpha \end{cases}, \tag{2}$$

where $f(i,j)$ is the grayscale value of the pixel in the grayscale image; $F(i,j)$ is the pixel value in a binary image, 0 or 1; and α is the threshold, value of 0.54.

Box-counting dimension of the fracture cracks

The fractal dimension is an important geometric feature of fractal theory that can describe the complexity of the fractal structure. In this paper, the fractal dimension of axial fracture crack is calculated by box dimension method. The larger the box dimension is, the more complicated the rock fracture cracks, and the higher the rock fragmentation. The slice diagram of the sample (as shown in Fig. 9 (a)) can be binarized to obtain a binarization image containing fractures, as shown in

Fig. 7 The relationship between the acoustic emission ringing counts, stress, and strain during the progressive failure process: (**a**) $T = 25\,°C$, (**b**) $T = 200\,°C$, (**c**) $T = 400\,°C$, (**d**) $T = 600\,°C$, (**e**) $T = 800\,°C$, and (**f**) $T = 1000\,°C$
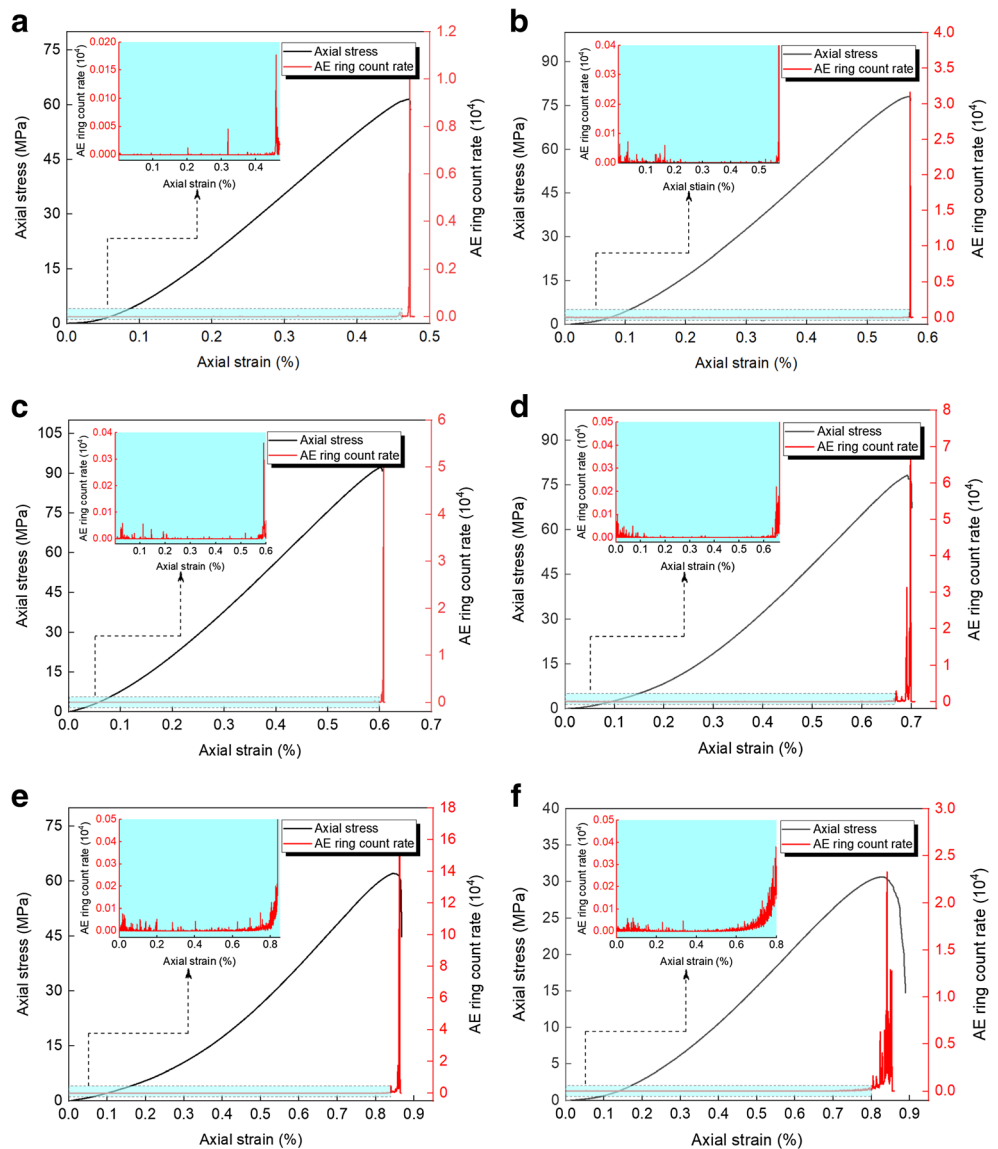

Fig. 9 (b). The binary image with fracture cracks is divided X ($0 \leq X \leq 8$) times by the MATLAB program, and the relative size of the "box" is 2^{-X}. After each bisection, whether there is the pixel point with a value of 0 in each equal area, the unit equal area containing the pixel point with a value of 0 is recorded as a "box," and the total number of "boxes" after each bisection is recorded as 2^Y. The bisection process is shown in Fig. 9.

$$log_2^{2^Y} = C - D log_2^{2^{-X}}, \tag{3}$$

where C is a constant and D is the box-counting dimension.
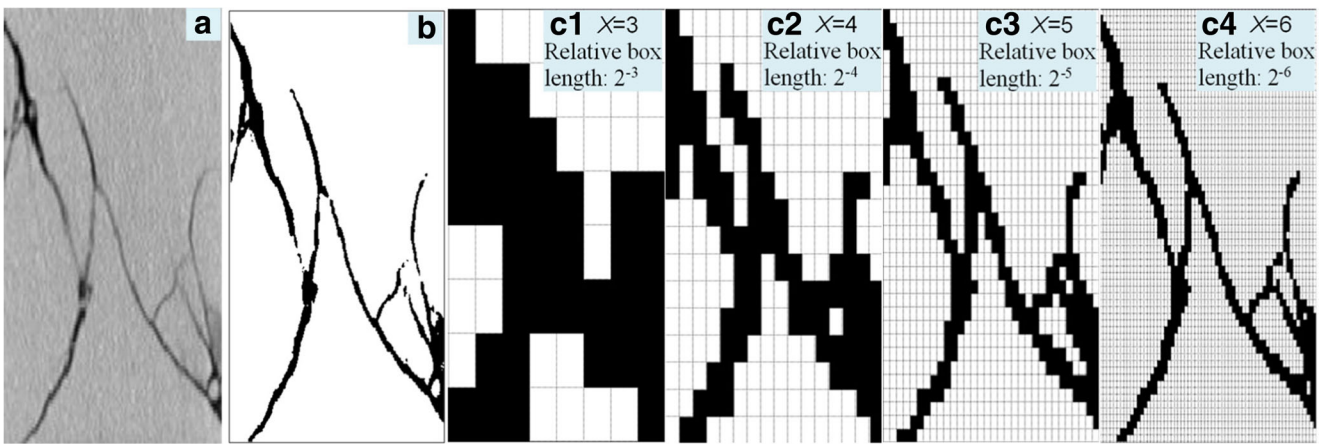
Fig. 8 Fracture cracks of typical samples
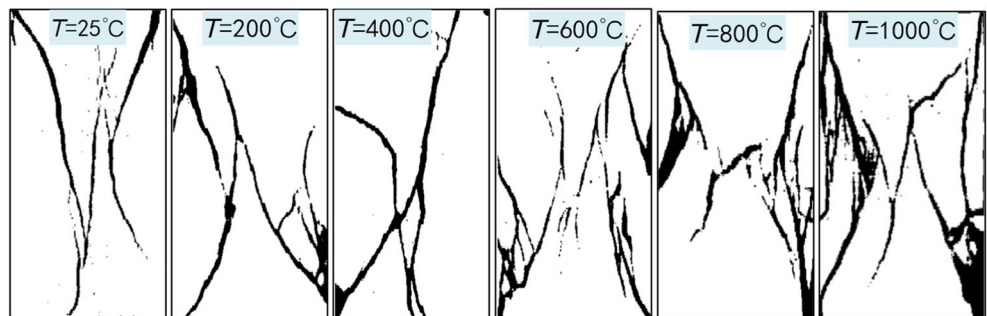
Fig. 9 Box dimension calculation: (**a**) CT image, (**b**) extracted crack, (**c1–c4**) example of box dimension test

By rearranging both sides of the equal sign of Eq.(3), Eq.(4) can be obtained as follows.

$$Y = C + DX \qquad (4)$$

According to Eq. (4), the linear relationship of X-Y in the Cartesian coordinate system is obtained. Linear fitting is carried out for different data points to obtain the linear relationship between each data point of rocks, as shown in Fig. 10. The slope of the fitted line is denoted as the fractal box-counting dimension D of the fracture crack. The fractal box-counting of the rock fractures varies with temperature, as shown in Fig. 11.

The box-counting dimensions of fracture crack of rock samples treated at 25, 200 and 400 °C were 1.4060, 1.4306, and 1.4626 respectively, showing a trend of increasing fractal

dimension with the increase of temperature. Compared with the sample at 25 °C, the box-counting dimension of the sample at 200 and 400 °C increases by 1.75 and 4.06%, respectively, with a small increase. When the heat treatment temperatures are 600, 800, and 1000 °C, the box-counting dimensions of fracture crack is 1.5155, 1.5817 and 1.7262, and the box-counting dimensions of the sample fracture crack increased rapidly with increasing temperature, which increased by 7.79, 12.50, and 22.77%, respectively, compared with the sample at 25 °C. When the temperature is 25–400 °C, the fracture crack mainly includes several obvious macroscopic fractures, and the higher the temperature, the more cracks there are. In addition, as shown in Fig.8, when the temperature exceeds 400 °C, the failure crack contains not only large continuous cracks but also some short, thick, and fine cross
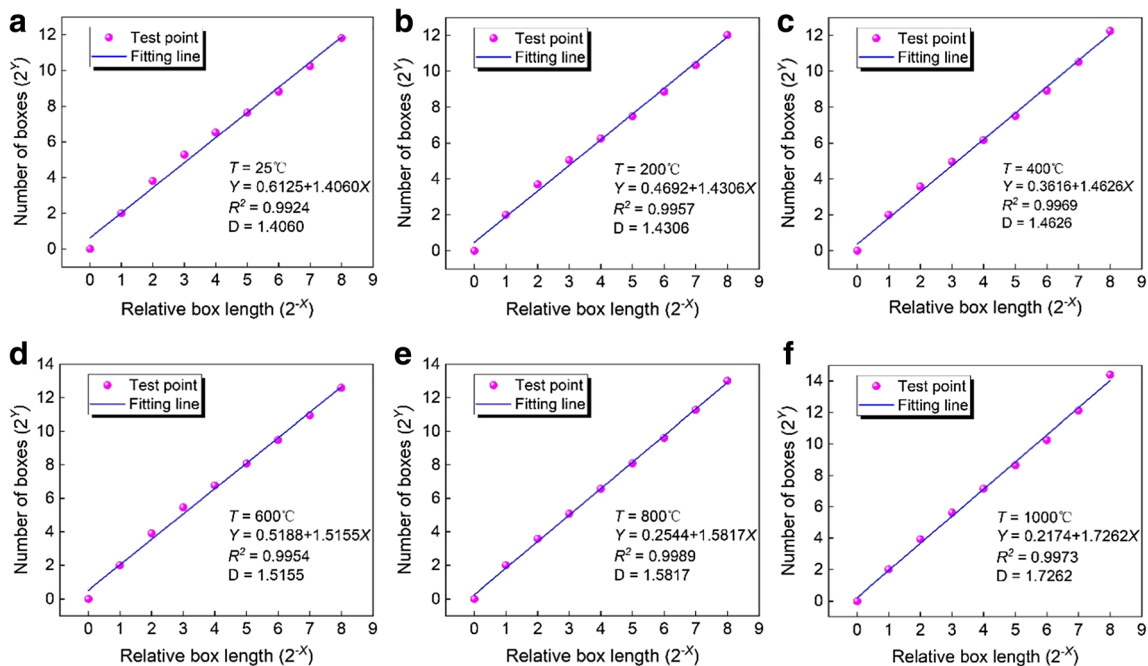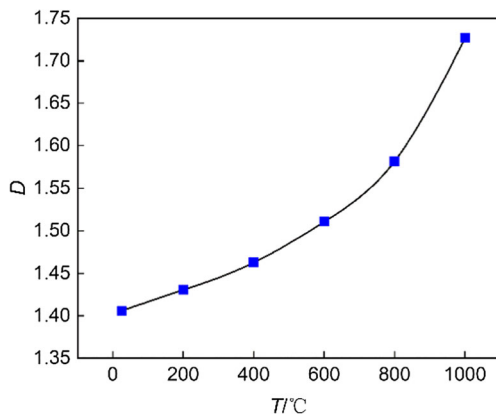

Fig. 10 Line fitting and box dimension

Fig. 11 Relationship between the box-counting dimension and temperature

cracks. The cross cracks are mainly concentrated in the middle of the sample, showing the distribution characteristics of increased crack density and enhanced connectivity. It can be seen that the damage and failure characteristics of rock samples at different temperatures are different in the uniaxial compression process and the temperature can increase the fracture crack complexity of the samples. Moreover, when the temperature exceeds 400 °C, the box dimension of the crack increases rapidly with the increase of the temperature, indicating that the high temperature above 400 °C can significantly enhance the complexity of rock crack.

Discussion on the temperature dependence

Sandstone samples are rock materials with pores in their natural state. The free and adsorbed water in the pores and the binding water between the mineral particles will gradually escape under the action of high temperature, resulting in great changes in the color, mass, and volume of the rock sample. In order to specifically analyze their change characteristics with temperature, the mass loss rate η_m and volume expansion rate η_V, respectively, are calculated as follows:

$$\eta_m = \frac{m_0 - m_1}{m_0} \times 100\%, \tag{5}$$

$$\eta_V = \frac{V_1 - V_0}{V_1} \times 100\%, \tag{6}$$

where η_m is the mass loss rate of the rock sample after high-temperature heating %; η_V is the volume expansion rate after high-temperature heating, %; m_0 and m_1 and V_0 and V_1 represent the mass and volume before and after high-temperature heating, respectively.

According to Eqs. (5) and (6), the η_m and η_v of all rock samples after the different high-temperature heating treatments are calculated, and the relationship curve between their average value and temperature is drawn, as shown in Fig. 12. Figure 12 shows that the mass loss rate and volume expansion

rate of the sample increase with increasing temperature. On the one hand, the combined water between the free water and the rock particles in the sample escapes at high temperature, which results in mass loss; on the other hand, the thermal expansion crack generated at high temperature causes volume expansion. After the high-temperature heating treatment, the change in the mass and volume of the sample will affect the strength characteristics of the rock sample under uniaxial compression. When experiencing temperatures of 200 and 400 °C, the free water and bound water between rock particles escape, which optimizes the contact effect between rock particles, enhances the friction force on the contact surface of rock particles, and significantly increases the compressive strength and deformation modulus of rocks, as shown in Fig. 3. When the temperature exceeds 400 °C, the expansion force of rock particles further increases with increasing temperature. When the expansion force exceeds the bearing capacity of the rock particles, cracks appear in the rock, and the mechanical properties of the rock deteriorate. Therefore, it can be clearly seen in Fig. 12 and Fig. 3 that the volume expansion rate of rock samples continues to increase and the peak stress gradually decreases after experiencing a temperature above 400 °C. The stress threshold of the rock stresses at different deformation stages shows a tendency of first increasing and then decreasing with the increasing temperature, and the peak is reached at 400 °C, as shown in Fig. 5.

The progressive failure process of rock is also the process of gradual deformation. Although all rock sample volumes are changed after high temperatures, the effects of the different temperatures on the deformation of rock are different. During the progressive failure process of the specimen, the crack growth volume is represented by the volume strain increment of the crack ($\Delta\varepsilon_{vcr}$) in the rock from the compaction point M of the crack volume to the peak stress point P, as shown in Fig. 4, and it is calculated as follows:

$$\Delta\varepsilon_{vcr} = \Delta\varepsilon_v^{cd} + \Delta\varepsilon_v^{cp}, \tag{7}$$
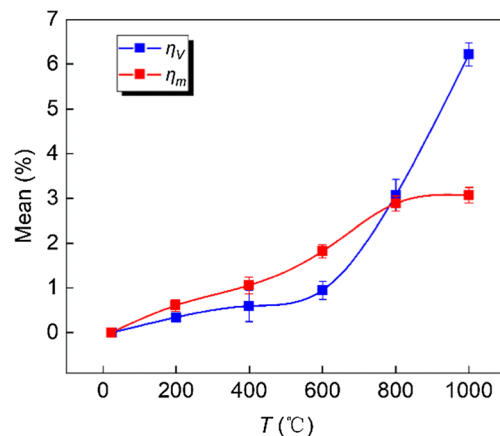
Fig. 12 The η_m and η_v of samples of different temperatures

Figure 13 shows the variation of the crack volume strain increment ($\Delta\varepsilon_{vcr}$) and the peak stress (σ_c) at different temperatures from 25 to 1000 °C during uniaxial compression. Through this analysis, it can be seen that the crack volume strain increment at 400 °C is the smallest, but the peak stress is the largest, which indicates that high temperature can enhance the brittleness of rock to some extent and weaken its resistance to deformation. It can also be seen from Fig. 7 that the AE ringing rate of rock samples experiencing heating from 25 to 400 °C increases rapidly at the peak stress point. This increase occurs because high temperature enhances the brittleness of rock to a certain extent, which makes the rock failure process complete immediately after the main fracture is through; in addition, a large number of acoustic emission signals are generated at the peak stress point. The failure samples are relatively complete, the complexity of failure cracks is low, and the box-counting dimension is small, as shown in Fig. 11. When the temperature is more than 400 °C, the brittleness of the rock gradually weakens, and the cracks in the rock gradually sprout and expand during the process of uniaxial compression. When the cracks reach a certain degree, macrofractures appear in the rock, which is a process of progressive development. The whole process is accompanied by the continuous generation of acoustic emission signals. At the same time, the continuous expansion of the internal crack makes the rock specimen crack increase obviously after the failure, the complexity of the crack is higher, and the box-counting dimension is larger. High-temperature heating has an important effect on the rock physical mechanics and deformation characteristics.

Conclusions

To investigate the strength and deformation failure characteristics of sandstones affected by temperature, including the stress threshold, sample volume strain, crack volume strain,
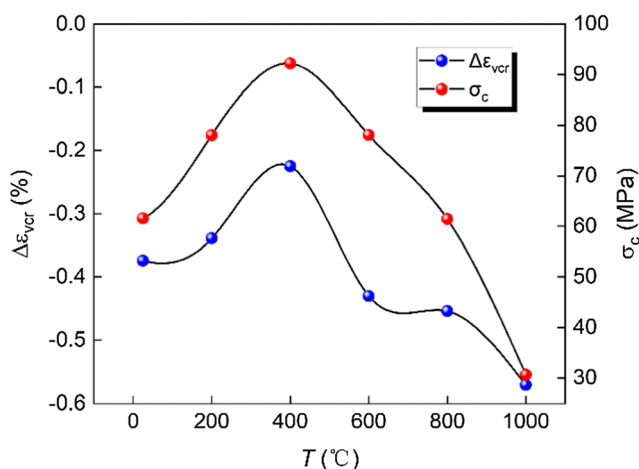
AE events, and distribution characteristics of fracture cracks. The uniaxial compression test of sandstone was carried out, and the internal structure of the damaged sample was observed by the CT test to study the distribution characteristics of fracture cracks. The main conclusions as follows:

(1) High-temperature heating has an important influence on the physical mechanics and deformation characteristics of rocks. On the one hand, with the increase of temperature, the free water and bound water gradually escape, the weight of the sample decreases, and the volume expands. On the other hand, the mechanical properties of rock show the characteristics of strengthening first and then weakening with the increase of temperature, in which 400 °C is the critical temperature of the process.

(2) The stress characteristic values, namely, σ_{cc}, σ_{ci}, σ_{cd}, and σ_c, can be used to divide the stress-strain curve into different deformation stages. And with the temperature increases, the stress thresholds first increase and then decrease gradually and reach the maximum value at 400 °C.

(3) Temperature changes the ductility of rock and affects the crack evolution during the progressive failure process. When the temperature is between 25 and 400 °C, the brittleness of the rock gradually increases after the high-temperature treatment, and the activity of AE signal increases sharply near the peak stress. When the temperature is between 400 and 1000 °C, the ductility of rock gradually increases, and the AE signal is gradually generated during the whole progressive failure process.

(4) With the influence of temperature, the rock fracture cracks gradually increase and gather in the middle of the specimen. And the fracture crack is widespread from a single penetrating crack to a small crack with a complex distribution, which the box dimension ranges from 1.4060 to 1.7262 and increases with the temperature.

Authors' contributions Dongming Zhang and Weijing Xiao conceived and designed the experiments; Han Yang and Xiaoming Li performed the experiments; Maolin Ye and Shujian Li analyzed the data; and Dongming Zhang and Weijing Xiao wrote the paper.

Compliance with ethical standards

Conflict of interest The authors declare no conflict of interest.

References

Ao H, Deng C, Dekkers M, Liu Q (2010) Magnetic mineral dissolution in pleistocene fluvio-lacustrine sediments, Nihewan Basin (North China). Earth Planet Sci Lett 292(1–2):191–200. https://doi.org/10.1016/j.epsl.2010.01.035

Fig. 13 Relationship between $\Delta\varepsilon_{vcr}$ and σ_c and temperature (*Note: The negative number represents the crack dilatation, not the numerical size*)

Araújo R, Sousa J, Bloch M (1997) Experimental investigation on the influence of temperature on the mechanical properties of reservoir rocks. Int J Rock Mech Min Sci 34(3-4):298.e1–298.e16. https://doi.org/10.1016/S1365-1609(97)00065-8

Chen T, Xu J, Liu S, Wang P, Fang X (2014) Experimental study on dynamic mechanical properties of post-high-temperature sandstone. Explos Shock Waves 34:195–201

Chen H, Zhang X, Yao C, Xia Z, Yang J, Jiang S, Jiang Q (2019a) Experimental and modeling research on heated rock fracture seepage. J China Coal Soc 44(9):2760–2766. https://doi.org/10.13225/j.cnki.jccs.2018.1217

Chen Z, He C, Xu G, Ma G, Wu D (2019b) A case study on the asymmetric deformation characteristics and mechanical behavior of deep-buried tunnel in phyllite. Rock Mech Rock Eng 52(4):4527–4545. https://doi.org/10.1007/s00603-019-01836-2

Cheon D, Jung Y, Park E, Song W, Jang H (2011) Evaluation of damage level for rock slopes using acoustic emission technique with waveguides. Eng Geol 121(1–2):75–88. https://doi.org/10.1016/j.enggeo.2011.04.015

Eberhardt E D (1998) Brittle rock fracture and progressive damage in uniaxial compression [Ph. D. Thesis]. Saskatoon, Sask:University of Saskatchewan

Feng Y, Harrison J, Bozorgzadeh N (2019) Uncertainty in in situ stress estimations: a statistical simulation to study the effect of numbers of stress measurements. Rock Mech Rock Eng 52:5071–5084. https://doi.org/10.1007/s00603-019-01891-9

Gaunt H, Sammonds P, Meredith P, Chadderton A (2016) Effect of temperature on the permeability of lava dome rocks from the 2004–2008 eruption of Mount St. Helens. Bull Volcanol 78(4):30. https://doi.org/10.1007/s00445-016-1024-5

Gong F, Wu W, Li T, Si X (2019a) Experimental simulation and investigation of spalling failure of rectangular tunnel under different three-dimensional stress states. Int J Rock Mech Min Sci 122:104081. https://doi.org/10.1016/j.ijrmms.2019.104081

Gong F, Yan J, Luo S, Li X (2019b) Investigation on the linear energy storage and dissipation laws of rock materials under uniaxial compression. Rock Mech Rock Eng 52(12):4237–4255. https://doi.org/10.1007/s00603-019-01842-4

Koprubasi N, Aldanmaz E (2004) Geochemical constraints on the Petrogenesis of Cenozoic I-type Granitoids in Northwest Anatolia, Turkey: evidence for magma generation by lithospheric delamination in a post-collisional setting. Int Geol Rev 46(8):705–729. https://doi.org/10.2747/0020-6814.46.8.705

Liu S, Xu J (2015) An experimental study on the physico-mechanical properties of two post-high-temperature rocks. Eng Geol 185:63–70. https://doi.org/10.1016/j.enggeo.2014.11.013

Liu Q, Qian Z, Wu Z (2017) Micro/macro physical and mechanical variation of red sandstone subjected to cyclic heating and cooling: an experimental study. Bull Eng Geol Environ 78:1485–1499. https://doi.org/10.1007/s10064-017-1196-z

Lu Y, Wang L, Sun X, Wang J (2016) Experimental study of the influence of water and temperature on the mechanical behavior of mudstone and sandstone. Bull Eng Geol Environ 76(2):1–16. https://doi.org/10.1007/s10064-016-0851-0

Lv J, Yu L, Du W, Li Q (2018) Theoretical approach of characterizing the crack-tip constraint effects associated with material's fracture toughness. Arch Appl Mech 88(9):1637–1656. https://doi.org/10.1007/s00419-018-1392-8

Manthei G (2005) Characterization of acoustic emission sources in a rock salt specimen under Triaxial compression. Bull Seismol Soc Am 95(5):1674–1700. https://doi.org/10.1785/0120040076

Martin C (1997) Seventeenth Canadian geotechnical colloquium:the effect of cohesion loss and stress path on brittle rock strength. Can Geotech J 34(5):698–725. https://doi.org/10.1139/cgj-34-5-698

Ohnaka M (1983) Acoustic emission during creep of brittle rock. Int J Rock Mech Min Sci Geomech Abstr 20(3):121–134. https://doi.org/10.1016/0148-9062(83)91302-5

Peng J, Rong G, Yao M, Wong L, Tang Z (2019) Acoustic emission characteristics of a fine-grained marble with different thermal damages and specimen sizes. Bull Eng Geol Environ 78:4479–4491. https://doi.org/10.1007/s10064-018-1375-6

Rabbani A, Baychev T, Ayatollahi S, Jivkov A (2017) Evolution of pore-scale morphology of oil shale during pyrolysis: a quantitative analysis. Transp Porous Media 119:143–162. https://doi.org/10.1007/s11242-017-0877-1

Rao Q, Wang Z, Xie H, Xie Q (2007) Experimental study of mechanical properties of sandstone at high temperature. J Cent S Univ Technol 14:478–483. https://doi.org/10.1007/s11771-007-0311-x

Rathnaweera T, Ranjith P, Gu X, Perera M, Kumari W, Wanniarachchi W, Haque A, Li J (2018) Experimental investigation of thermomechanical behaviour of clay-rich sandstone at extreme temperatures followed by cooling treatments. Int J Rock Mech Min Sci 107:208–223. https://doi.org/10.1016/j.ijrmms.2018.04.048

Saif T, Lin Q, Bijeljic B, Blunt M (2017) Microstructural imaging and characterization of oil shale before and after pyrolysis. Fuel 197:562–574. https://doi.org/10.1016/j.fuel.2017.02.030

Singh S (2019) Protracted zircon growth in migmatites and In situ melt of Higher Himalayan Crystallines:U-Pb ages from Bhagirathi valley, NW Himalaya, India. Geosci Front 10(3):8–24. https://doi.org/10.1016/j.gsf.2017.12.014

Song Z, Ji H, You S, Tan J, Wang H (2018) Experimental study on sensitivity to temperature stress of the permeability of weakly cemented sandstone. Iop Conference 113:012120. https://doi.org/10.1088/1755-1315/113/1/012120

Tang S, Zhang H, Tang C, Liu H (2015) Numerical model for the cracking behaviour of heterogeneous brittle solids subjected to thermal shock. Int J Solids Struct 80:520–531. https://doi.org/10.1016/j.ijsolstr.2015.10.012

Wang X, Wen Z, Jiang Y, Huang H (2017) Experimental study on mechanical and acoustic emission characteristics of rock-like material under non-uniformly distributed loads. Rock Mech Rock Eng 51:729–745. https://doi.org/10.1007/s00603-017-1363-3

Wang G, Yang D, Kang Z (2020) Experimental study on anisotropic permeability of oil shale under high temperature and triaxial stress. Chin J Rock Mech Eng 39(6):1129–1141. https://doi.org/10.13722/j.cnki.jrme.2019.0863

Xiao W, Zhang D, Cai Y, Chu Y (2020) Study on loading rate dependence of the coal failure process based on uniaxial compression test. Pure Appl Geophys. https://doi.org/10.1007/s00024-020-02513-0

Xie Y, Shan Y, Li X, Zhou W, Tong C, Wang L (2015) Experimental study on effects of temperature and stress on properties of reservoir rocks in Yinggehai and Qiongdongnan basin, South China Sea. J Chengdu Univ Technol Sci Technol Ed 42(2):218–224. https://doi.org/10.3969/j.issn.1671-9727.2015.02.10

Yang S (2015) Fracture mechanical behavior of red sandstone containing a single fissure and two parallel fissures after exposure to different high-temperature treatments. In: Strength Failure and Crack Evolution Behavior of Rock Materials Containing Pre-existing Fissures. Springer Environmental Science and Engineering. Springer, Berlin, Heidelberg 157–183. https://doi.org/10.1007/978-3-662-47303-0_7

Yang S, Xu P, Li Y, Huang Y (2017) Experimental investigation on triaxial mechanical and permeability behavior of sandstone after exposure to different high temperature treatments. Geothermics 69:93–109. https://doi.org/10.1016/j.geothermics.2017.04.009

Yang S, Yin P, Huang Y (2019) Experiment and discrete element modelling on strength, deformation and failure behaviour of shale under brazilian compression. Rock Mech Rock Eng 52(7):4339–4359. https://doi.org/10.1007/s00603-019-01847-z

You S, Ji H, Wang T, Song Z (2018) Thermal and mechanical coupling effects on permeability of weakly cemented sandstone. Emerg Mater Res 7(2):100–108. https://doi.org/10.1680/jemmr.16.00082

Yushi Z, Shicheng Z, Tong Z, Xiang Z, Tiankui G (2016) Experimental investigation into hydraulic fracture network propagation in gas shales using CT scanning technology. Rock Mech Rock Eng 49(1):33–45. https://doi.org/10.1007/s00603-015-0720-3

Zhang P, Mishra B, Heasley K (2015) Experimental investigation on the influence of high pressure and high temperature on the mechanical properties of deep reservoir rocks. Rock Mech Rock Eng 48(6):2197–2211. https://doi.org/10.1007/s00603-015-0718-x

Zhang W, Sun Q, Zhu Y, Guo W (2018) Experimental study on response characteristics of micro–macroscopic performance of red sandstone after high-temperature treatment. J Therm Anal Calorim 136:1935–1945. https://doi.org/10.1007/s10973-018-7880-9

Zhao Y, Wan Z, Feng Z, Xu Z, Liang W (2017) Evolution of mechanical properties of granite at high temperature and high pressure. Geomech Geophys Geo-Energy Geo-Rresour 3(2):199–210. https://doi.org/10.1007/s40948-017-0052-8